

## Crystallographic and Functional Studies of a Modified Form of Eosinophil-derived Neurotoxin (EDN) with Novel Biological Activities

Changsoo Chang<sup>1</sup>, Dianne L. Newton<sup>2</sup>, Susanna M. Rybak<sup>3</sup> and Alexander Wlodawer<sup>1\*</sup>

<sup>1</sup>Macromolecular Crystallography Laboratory National Cancer Institute Frederick, MD 21702, USA

<sup>2</sup>SAIC Frederick, National Cancer Institute, Frederick MD 21702, USA

<sup>3</sup>Developmental Therapeutics Program, National Cancer Institute, Frederick, MD 21702, USA

The crystal structure of a post-translationally modified form of eosinophil-derived neurotoxin (EDN) with four extra residues on its N terminus ((-4)EDN) has been solved and refined at atomic resolution (1 Å). Two of the extra residues can be placed unambiguously, while the density corresponding to two others is poor. The modified N terminus appears to influence the position of the catalytically important His129, possibly explaining the diminished catalytic activity of this variant. However, (-4)EDN has been shown to be cytotoxic to a Kaposi's sarcoma tumor cell line and other endothelial cell lines. Analysis of the structure and function suggests that the reason for cytotoxicity is most likely due to cellular recognition by the N-terminal extension, since the intrinsic activity of the enzyme is not sufficient for cytotoxicity and the N-terminal extension does not affect the conformation of EDN.

**Keywords:** crystal structure; atomic resolution; cytotoxic ribonuclease; Kaposi sarcoma; active site

\*Corresponding author

### Introduction

Biological actions reported for human ribonucleases (RNases) homologous to RNase A range from the causation of neurological symptoms in animal models to host defense actions and neovascularization.<sup>1–3</sup> Human RNases present therapeutic opportunities for cancer and viral diseases. Eosinophil-derived neurotoxin (EDN) is one of the major proteins present in the granules of eosinophils. Recent results indicate that EDN may possess activity directed against respiratory syncytial virus (RSV) through direct inhibition of RSV replication.<sup>4</sup> These results led to the hypothesis that RNases have evolved antiviral host defense activity.

A novel post-translationally modified form of EDN (called (-4)EDN) contains amino acid residues -4 to -1 of the EDN signal peptide.<sup>5</sup> The post-translationally modified (-4)EDN was

reported to inhibit oocyte maturation<sup>5</sup> and to be present predominantly in pregnant women.<sup>6</sup> The -4 to -1 amino acid sequence (SLHV) resembles a peptide reported to recognize Kaposi's sarcoma (KS) tumors *in vivo*.<sup>7</sup> EDN genetically modified to express the four amino acid extension was cytotoxic to an endothelial-like KS cell-line (KS Y-1)<sup>8</sup> and other endothelial cell lines.<sup>9</sup> Since small peptides can target drugs,<sup>7</sup> the four amino acid peptide extension might act as a recognition motif for a receptor-like molecule on some cells, effectively targeting EDN to that cell. It may be responsible for some of the anti-KS activity<sup>8</sup> previously associated with a human pregnancy hormone (hCG).<sup>10</sup>

A crystal structure of the native form of EDN has been reported at 1.83 Å resolution,<sup>11</sup> although the coordinates resulting from that work have not been made publicly available. More recently, structures of three complexes of that enzyme with nucleotides, as well as of EDN with only a sulfate ion bound in the active site, were published at 1.8–1.6 Å resolution.<sup>12</sup> The studies reported here provide the first glimpse at this enzyme at an atomic resolution, and compare the enzymatic and biological activities of the native enzyme and its extended form.

Abbreviations used: EDN, eosinophil-derived neurotoxin; KS, Kaposi's sarcoma; RI, placental ribonuclease inhibitor; PEG, polyethylene glycol.

E-mail address of the corresponding author: [wlodawer@ncicrf.gov](mailto:wlodawer@ncicrf.gov)

**Table 1.** Data collection statistics

Wavelength (Å)	0.98
Space group	$P2_12_12_1$
Unit cell parameters (Å)	$a = 42.14$ $b = 52.56$ $c = 56.63$
Resolution (Å)	20–1.0
Total no. of reflections	495,612
Unique reflections	62,494
Completeness (last shell) (%)	90.9 (76.4)
$R_{\text{merge}}$ (%)	2.6 (20.1)

$R_{\text{merge}} = \sum |I_i - \langle I_i \rangle| / \sum I_i$ , where  $I_i$  is the intensity measurement for reflection  $i$ , and  $\langle I_i \rangle$  is the mean intensity calculated for reflection  $i$  from replicate data.

## Results and Discussion

Diffraction data for (−4)EDN were collected using synchrotron radiation at 1 Å resolution (Table 1). The structure was solved by molecular replacement using the coordinates of EDN as the starting model.<sup>11</sup> The structure was refined with the application of anisotropic temperature factors and the final coordinates discussed below, as well as the structure factors, have been deposited with the Protein Data Bank (see Materials and Methods).

### Assessment of the quality of the refined structure

The final refined model of (−4)EDN contains 136 amino acid residues, two sulfate ions, and 244 water molecules. The  $R$ -value for all reflections in the 20.0–1.0 Å range is 13.2% ( $R_{\text{free}}$  of 16.9%). The refinement statistics are summarized in Table 2. All residues except for glycine or proline lie either in the most-favored or in additionally allowed regions of the Ramachandran plot.<sup>13</sup> The electron density map is very clear, except in the N-terminal region and in a few flexible regions. The first residue that can be traced unambiguously is His −2. Although weak density appeared on the amino side of this residue, the peptide bond between residues −3 and −2 is energetically unfavorable in the Ramachandran plot when the main chain for residues −4 to −2 was built along that density. Thus, the first two residues were not included in the final model, which consists of the uninterrupted chain extending from His −2 to Ile134. Besides at the N terminus, the electron density map in the vicinity of Lys66 and Gln91 is not clear (reasonably well defined for the main chain, but absent for the side-chain atoms). These residues are located in rather flexible regions, as judged by their comparatively high temperature factors. The average  $B$ -factors of the main-chain atoms for residues Ser64, Asn65, Lys66, Pro90, Gln91, Asn92 are 27.0 Å<sup>2</sup>, 34.0 Å<sup>2</sup>, 32.5 Å<sup>2</sup>, 31.0 Å<sup>2</sup>, 37.0 Å<sup>2</sup>, and 29.5 Å<sup>2</sup>, respectively, whereas the respective average  $B$ -factors of the side-chain atoms for these residues are 32.7 Å<sup>2</sup>, 49.2 Å<sup>2</sup>, 73.4 Å<sup>2</sup>, 39.7 Å<sup>2</sup>, 70.2 Å<sup>2</sup>, and 47.6 Å<sup>2</sup>. In the structure of RNase A, the residue correspond-

**Table 2.** Refinement statistics

Resolution range (Å)	20.0–1.0
Reflections used	62,423
$R_{\text{cryst}}$ <sup>a</sup> (%)	13.2
$R_{\text{free}}$ <sup>b</sup> (%)	16.9
R.m.s. deviations from ideality	
Bond lengths (Å)	0.036
Angles (Å)	0.047
Average $B$ -factor (Å <sup>2</sup> )	
All atoms <sup>c</sup>	20.32
Main chain atoms <sup>c</sup>	12.66
Side-chain atoms <sup>c</sup>	20.38
Solvent atoms	35.08
Hetero atoms	28.06
No. protein atoms	1168
No. solvent atoms	244
No. hetero atoms	10

<sup>a</sup>  $R_{\text{cryst}} = \sum ||F_o| - |F_c|| / \sum |F_o|$ .

<sup>b</sup>  $R_{\text{free}}$  is the cross validation  $R_{\text{cryst}}$  computed for the test set of reflections (5% of all reflections) which were omitted from the refinement process.

<sup>c</sup> For protein atoms, the  $B$ -factor was averaged for all atoms, including hydrogen atoms.

ing to Asn65 in (−4)EDN is Asn67. That residue can be deamidated easily under mild conditions and converted to iso-Asp, and it was shown to be highly flexible in the ultrahigh-resolution structure of RNase A.<sup>14</sup> The  $B$ -factor for the C-terminal residue Ile134 is also high. The electron density map for the main-chain atoms of that residue is defined well, but not very clear for the side-chain atoms, especially CD1 and CG2.

### Overall structure and multiple conformations of the side-chains

The overall structure of (−4)EDN is virtually the same as that of EDN. When C<sup>α</sup> atoms for (−4)EDN and EDN (PDB accession code 1HI2<sup>12</sup>) are superimposed, the r.m.s. deviation is 0.29 Å. The overall shape of (−4)EDN shows the typical RNase fold, which is a V-shaped  $\alpha + \beta$ -type polypeptide with the active-site cleft in the middle. The secondary structure elements correspond to those described for EDN, consisting of six  $\beta$  strands and four  $\alpha$  helices (including one  $3_{10}$  helix). The structure of (−4)EDN is organized into two lobes with the two N-terminal  $\alpha$  helices ( $\alpha_1$  and  $\alpha_2$ ) located between them. Strands  $\beta_1$ ,  $\beta_3$ , and  $\beta_4$  create an anti-parallel  $\beta$  sheet in one of the lobes, and a  $3_{10}$  helix between  $\beta_3$  and  $\beta_4$  belongs to the same lobe. The other lobe is composed of the helix  $\alpha_3$  and an anti-parallel  $\beta$  sheet composed of strands  $\beta_2$ ,  $\beta_5$ , and  $\beta_6$  (Figure 1). EDN and (−4)EDN contain four disulfide bonds.

An interesting feature of this atomic-resolution structure is a large number of residues for which alternative conformations of their side-chains can be assigned. Such alternative conformations can be seen clearly for 18 residues (Table 3). By comparison, the structure of phosphate-free bovine pancreatic RNase A solved at 1.26 Å resolution shows

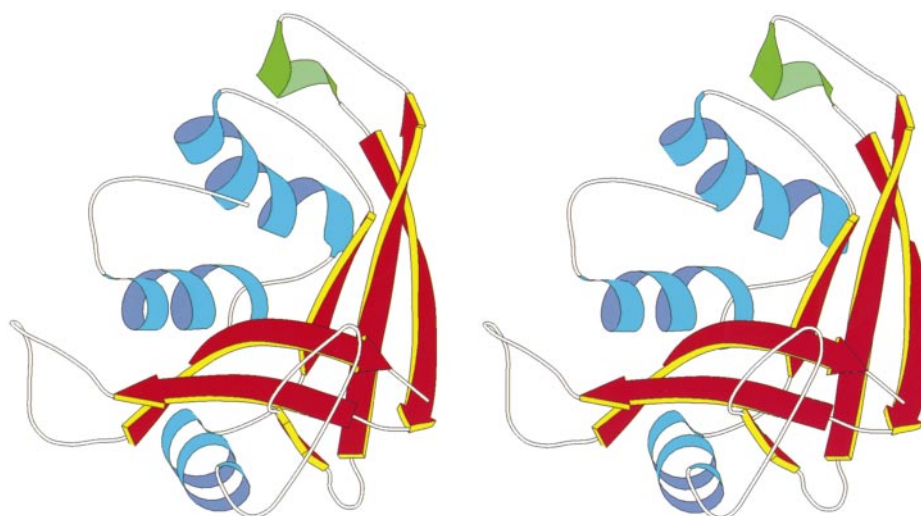


**Figure 1.** A stereo ribbon diagram of the (-4)EDN. Colors denote secondary structure elements, with  $\alpha$  helices shown in blue,  $\beta$  strands in red, and a  $3_{10}$  helix in green.

13 residues with alternative conformations.<sup>15</sup> However, the residues with multiple conformations are quite different in these two enzymes. In (-4)EDN,

such residues are distributed evenly throughout the molecule. The two alternative conformations of Gln40 and His82 are correlated in the same mol-

**Table 3.** Parameters for the residues showing alternate conformations

Residue	Number	Occupancy	Temperature factor ( $\text{\AA}^2$ )	$\chi_1$ (deg.)	$\chi_2$ (deg.)	$\chi_3$ (deg.)	$\chi_4$ (deg.)	$\chi_5$ (deg.)
Phe	5A	0.54	14.94	-72	87			
	5B	0.46	16.56	-56	129			
Gln	22A	0.54	12.32	-65	-66	-47		
	22B	0.46	13.56	-165	-112	-162		
Asn	25A	0.64	22.35	-66	-21			
	25B	0.36	29.43	-172	-61			
Ile	30A	0.75	14.34	-67	170			
	30B	0.25	10.18	-67	53			
Asn	32A	0.62	17.21	-79	-22			
	32B	0.38	25.69	-180	106			
Arg	36A	0.47	21.67	68	-169	-87	-80	0
	36B	0.53	23.42	56	180	-154	94	0
Asn	39A	0.59	19.56	-161	48			
	39B	0.41	18.74	-57	-67			
Gln	40A	0.69	23.40	177	-64	148		
	40B	0.31	22.31	50	-170	151		
Met	60A	0.47	20.92	59	179	-75		
	60B	0.53	31.89	82	175	-5		
Arg	68A	0.72	28.78	-75	-39	-61	-83	-1
	68B	0.28	26.43	-52	-80	-169	68	0
Ile	81A	0.80	17.67	-59	165			
	81B	0.20	29.50	-59	-47			
His	82A	0.69	16.39	-61	-64			
	82B	0.31	18.24	-161	52			
Ile	93A	0.38	40.74	-72	-16			
	93B	0.62	27.06	-72	168			
Gln	100A	0.54	14.92	178	159	-2		
	100B	0.46	11.62	60	-113	-28		
Val	109A	0.68	10.96	63				
	109B	0.32	10.48	-93				
Asp	115A	0.61	14.94	-171	76			
	115B	0.39	16.56	174	143			
Pro	120A	0.61	19.20	25	-37			
	120B	0.39	20.50	-26	45			
His	129A	0.61	16.19	-63	-66			
	129B	0.39	16.58	178	97			

Temperature factors are averaged for all atoms belonging to each alternate conformation.

ecule, while crystallographic contacts are responsible for the correlation between the alternative conformations of Phe5 and Gln22 (Figure 2).

One of the residues observed in two conformations is the active-site His129 (corresponding to His119 in RNase A). Several crystallographic stu-

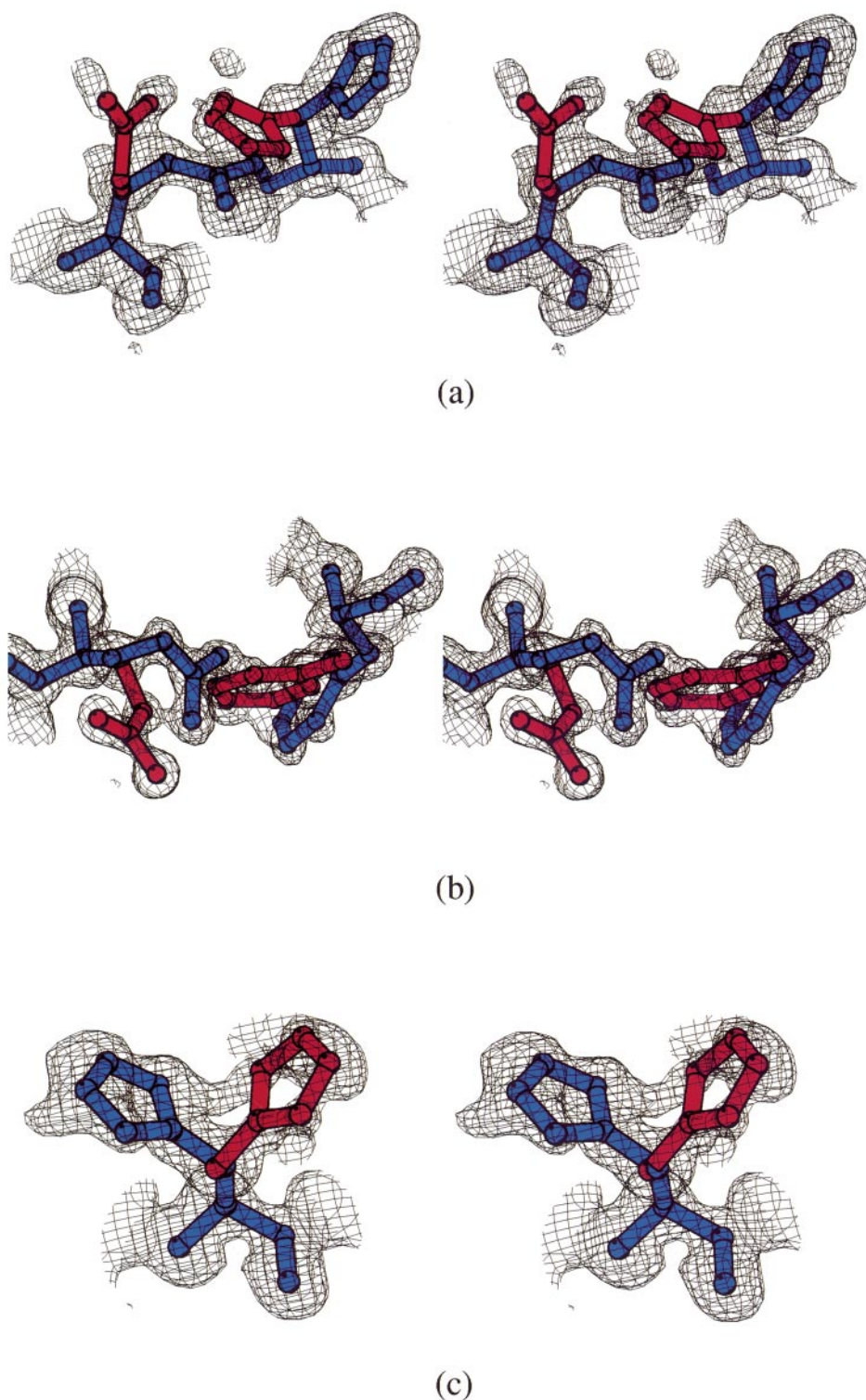


**Figure 2.** The  $2F_o - F_c$  density map for dual conformations of selected residues in (-4)EDN. (a) Residues Gln40 and His82; (b) residues Phe5 and Gln22; (c) His129. Each conformation is presented in a different color. Conformation A of Gln40 occupies the space for conformation B of His82. Conformation A of Phe5 occupies the space for conformation B of Gln22. The electron density was calculated with SHELXPRO and contoured at  $1.2 \sigma$ . Occupancies of each conformation are shown in Table 2.

dies of the latter enzyme have reported two distinct conformations for His119,<sup>14,16</sup> and the two conformations of His129 in (-4)EDN are closely similar to those in RNase A (Figure 2). As discussed further below, only one of these conformations agrees with the postulated enzymatic mechanism for this family of enzymes, while the second one is probably transient and does not support enzymatic activity.<sup>17</sup> For several other residues, the density for the alternative conformation is not ideal, but if only one conformation was included in the refinement, the resulting  $F_o - F_c$  map showed significant peaks that could not be due to solvent, since they were much too close to the protein chain. Examples of such residues are Asn25, Asn32, Gln40, Arg68, and His82.

### Substrate-binding pocket and the active-site residues

Since the recently solved structures of nucleotide complexes of EDN<sup>12</sup> were not available when the work described here was underway, the structure of a putative complex of (-4)EDN with a substrate was modeled (Figure 3) on the basis of the inactive conformation of RNase A as seen in the complex with (Tp)<sub>4</sub> (PDB accession code 1RTA<sup>18</sup>). The cleavage site of this substrate lies between nucleotides T3 and T4. In the (-4)EDN/substrate model, His -2, Arg36, and His129 seem to interfere with the binding of the substrate. His -2 and His129 are in contact with the base of T4. For the RNase A family, the structure with a sulfate ion shows that the side-chain of His129 (119 in RNase A) occupies that space.<sup>14,16</sup> Side-chain atoms of Arg36 (Arg39 in RNase A) occupy the same space as the

phosphate group of T1. Since the arginine side-chain can be flexible and thus be pushed away from the catalytic center, we may conclude that Arg36 is most likely not critical for substrate binding and should not affect reaction kinetics. The backbone atoms of Arg36 are located in the same area as in the RNase/substrate complex structure.

Two sulfate ions were found in the structure of (-4)EDN, and their locations are in agreement with the data reported recently for EDN with a sulfate ion bound in the active site.<sup>12</sup> Both of these sulfate ions are located in the substrate-binding pocket. Sul151 is conserved in the structures of other RNases and shows a hydrogen-bonding pattern similar to that of a T4 phosphate group in the complex discussed above. This sulfate ion makes hydrogen bonds with His15, His129, and the amide nitrogen atom of Leu130. For His129, both the "active" and the "inactive" conformations make hydrogen bonds with the sulfate ion. Besides these protein residues, four more water molecules interact with this sulfate ion. Sul152 is conserved in the EDN structures, but has not been found in the corresponding structures of RNase A. Sul152 does not show any special relationship to the substrate as defined above. This sulfate ion makes hydrogen bonds with the side-chain nitrogen atoms of Arg36 and Asn39B, while it does not make hydrogen bonds with Asn39A. The side-chain amide group of Gln40 also makes a hydrogen bond with Sul152. These hydrogen bonds are conserved in all sulfate-binding EDN structures.

The active-site residues of (-4)EDN include His15, Lys38, and His129 (His12, Lys41, and His119 in RNase A, respectively) and all of them are strictly conserved in RNase A. In the structures

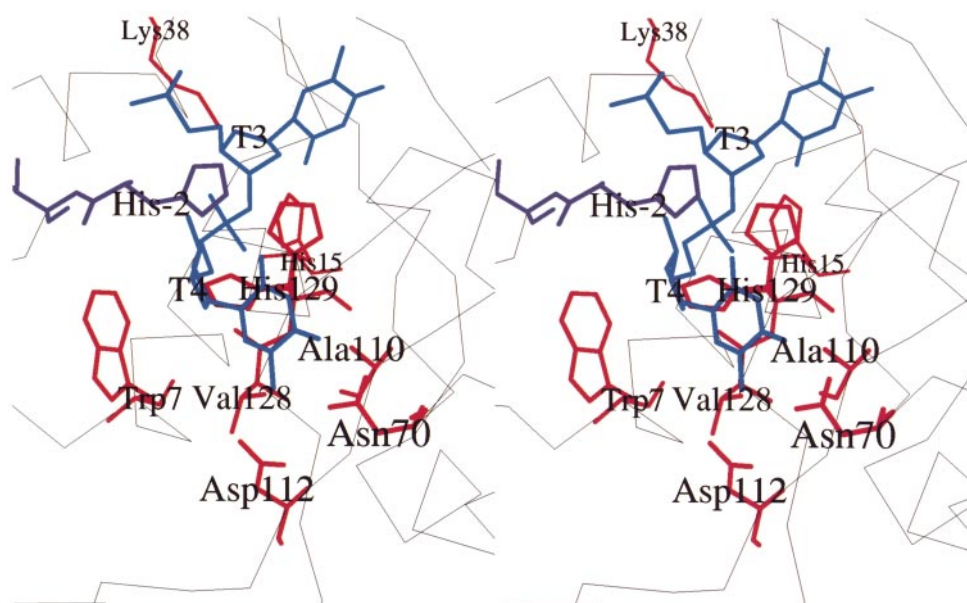


**Figure 3.** The active site of (-4)EDN. Active-site residues are presented in red, the substrate model is in blue, and His -2 is shown in magenta. Only the residues T3 and T4 of the substrate are displayed in the active site of the enzyme.

of RNase A, His119 has been reported in two conformations, denoted A ( $\chi_1 \approx 150^\circ$ ) and B ( $\chi_1 \approx -60^\circ$ ). Conformation A is compatible with nucleotide binding,<sup>19-21</sup> whereas low pH or the presence of sulfate/phosphate in the active site favors conformation B.<sup>14,22</sup> The high-resolution structure of (-4)EDN contains both of these conformations of His129. The occupancy of conformation B is 0.61 with an average *B*-factor of 16.2 Å<sup>2</sup>, whereas the occupancy of conformation A is 0.39 with an average *B*-factor of 16.6 Å<sup>2</sup>.

The residues that extend the N-terminal section of (-4)EDN are located near the active site of the enzyme. His - 2 is oriented toward the active site, while the additional N-terminal residues surround the substrate-binding pocket (Figure 3). His - 2 interacts with the catalytically important His129. This interaction might affect the relative occupancy of both observed conformations of His129 and thus explain the reduced enzymatic activity of (-4)EDN (see below). The side-chain of His - 2 is stabilized by this interaction and shows well-defined electron density, while the density corresponding to the first two residues (Ser - 4, Leu - 3) was so poor that we did not attempt to model them.

### Enzymatic activity

The enzymatic activity of (-4)EDN was compared to that of EDN (Table 4). While the affinities of both enzymes for a substrate were similar ( $K_m$  12.8 and 15.3 μM for EDN and (-4)EDN, respectively), the catalytic efficiency of (-4)EDN was only 8% that of EDN ( $K_{cat}/K_m$  ratio  $3.2 \times 10^6 \text{ M}^{-1} \text{ s}^{-1}$  versus  $2.5 \times 10^5 \text{ M}^{-1} \text{ s}^{-1}$ , EDN and (-4)EDN, respectively). The pH profiles of both enzymes were the same (not shown) and the optimal enzymatic activity was achieved at pH 7.5. Placental ribonuclease inhibitor (RI) inhibits a wide variety of pancreatic-type RNases<sup>23</sup> and we could confirm that the RNase activity of both EDN and (-4)EDN was inhibited by RI (Figure 4). Thus, appending four amino acid residues to the N terminus of EDN does not affect the pH at which ribonuclease activity is maximal, inhibition by RI, or the affinity of the enzyme for the substrate. However, the catalytic efficiency of the enzyme is diminished by an order of magnitude.

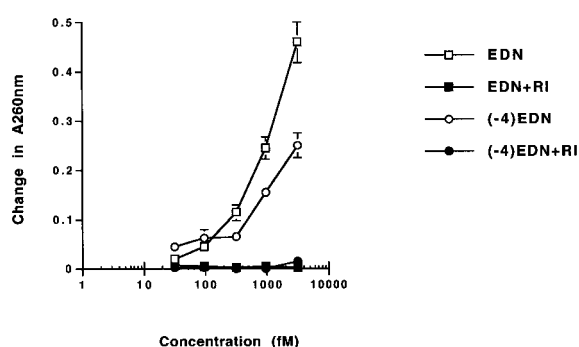


**Figure 4.** Inhibition of RNase activity by ribonuclease inhibitor (RI). Acid-soluble tRNA fragments were measured as described in Materials and Methods. Assays were performed in the absence of RI (open symbols) or the presence of 300 units/ml of RI (filled symbols). The data from two experiments were pooled and plotted. The tRNA concentration was 0.3 mg/ml. Standard errors of the means are shown when they are greater than the symbol. EDN, squares; (-4)EDN, circles.

### Binding of EDN and (-4)EDN to KS Y-1 cells

Previously, (-4)EDN was shown to inhibit the cell viability of KS Y-1 cells markedly, while EDN had no effect on viability.<sup>8</sup> KS Y-1 cells are a Kaposi's sarcoma-derived cell line.<sup>24</sup> The reported values of  $IC_{50}$  were 6 μg/ml and >100 μg/ml for (-4)EDN and EDN, respectively. Human pancreatic type RNases are generally not cytotoxic to cultured cells, but are as potent as toxins when injected into cells directly.<sup>25</sup> This one and other studies<sup>26</sup> indicate that transmembrane transport is rate-limiting for the expression of cytotoxicity by RNases. Moreover, peptides can bind to specific sites in order to deliver drugs.<sup>7</sup> Therefore, the possibility that the SLHV peptide could deliver EDN to an intracellular target by altering binding and internalization was investigated. Increasing concentrations of [<sup>125</sup>I]EDN and [<sup>125</sup>I](-4)EDN were incubated with KS Y-1 cells for two hours at 4 °C in the presence or absence of the respective unlabeled proteins. Binding of (-4)EDN was saturable (Figure 5(a)). In contrast, the binding of EDN did not appear to be saturable and continued to rise even at the highest concentration tested (1000 nM, Figure 5(b)). Interestingly, although the

**Table 4.** Kinetic parameters of EDN and (-4)EDN with tRNA as substrate

RNase	$K_m$ (μM)	$K_{cat}$ (s <sup>-1</sup> )	$K_{cat}/K_m$ (M <sup>-1</sup> s <sup>-1</sup> )
EDN	12.8	41	$3.2 \times 10^6$
(-4)EDN	15.3	3.7	$2.5 \times 10^5$ (8) <sup>a</sup>

The RNase activity was measured at pH 7.5 as described in Materials and Methods. The data were derived from the initial rates of reactions containing 31 fM EDN or 310 fM (-4)EDN and varying the concentrations of yeast tRNA substrate from 0.1 to 1 mg/ml.

<sup>a</sup> The number in parentheses indicates the percentage activity compared with EDN.

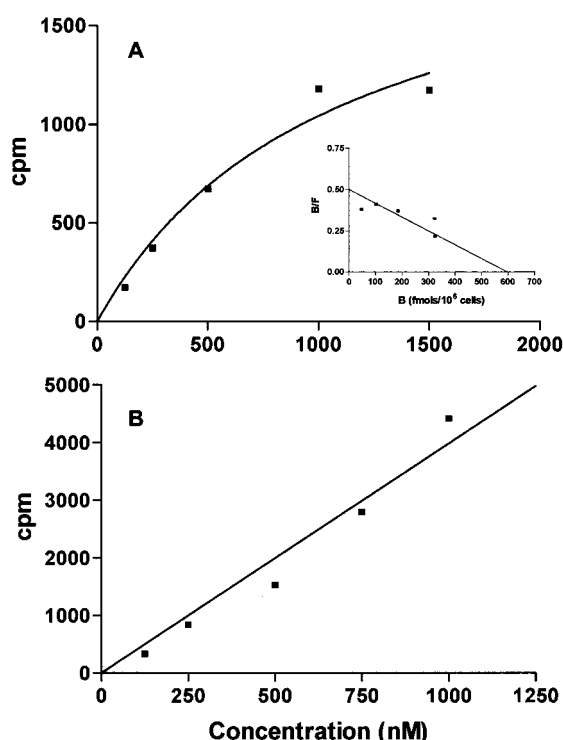


**Figure 5.** Binding of [<sup>125</sup>I]EDN and [<sup>125</sup>I](-4)EDN to KS Y-1 cells. The indicated concentrations of radiolabeled (a) (-4)EDN and (b) EDN were incubated with KS Y-1 cells for two hours at 4°C as described in Materials and Methods. Cell-associated radioactivity was determined by subtracting non-specific binding from total radioactivity bound. Inset: Scatchard analysis of the binding data obtained for (-4)EDN. B, bound; F, free. The specific activity of (-4)EDN and EDN was  $2.6 \times 10^6$  cpm/ $\mu$ g and  $2.0 \times 10^6$  cpm/ $\mu$ g, respectively.

specific activities of the two RNases were similar ( $2.0 \times 10^6$  cpm/ $\mu$ g and  $2.6 \times 10^6$  cpm/ $\mu$ g for EDN and (-4)EDN, respectively), the amount of radioactivity associated with the cell was approximately three- to fourfold higher for EDN than for (-4)EDN. Scatchard analysis of the saturable (-4)EDN binding indicated that it bound to cells with a  $K_D$  of about 1  $\mu$ M. This is close to the low-affinity binding reported for onconase on 9L glioma cells ( $0.25 \mu$ M<sup>26</sup>). Onconase is similar to other amphibian members of the pancreatic RNase A family that possess inherent cytotoxicity.<sup>27</sup> Cell-surface binding and internalization are involved in onconase cytotoxicity and, although the nature of the onconase receptor is not known,<sup>28</sup> we reasoned that the SLHV peptide might recognize a binding site similar to that of onconase. Competition binding experiments support this supposition, as onconase competed effectively for binding of [<sup>125</sup>I](-4)EDN but not of [<sup>125</sup>I]EDN. A 100-fold molar excess of unlabeled onconase diminished binding of 100 nM (-4)EDN to the same extent as a 44-fold molar excess of unlabeled (-4)EDN (Figure 6). Binding of 50 nM and 500 nM radio-

labeled (-4)EDN was also decreased (Figure 6). Although binding of radiolabeled EDN was decreased in the presence of the unlabeled enzyme, the presence of onconase had no effect on binding (Figure 6, top panel). These results indicate that (-4)EDN may be binding to the same or similar cell-surface sites as onconase, causing an alteration in cellular routing or processing that results in cytotoxicity.

### Intracellular processing of EDN and (-4)EDN in KS Y-1 cells

In view of the previous results, intracellular processing was examined to determine if the SLHV peptide alters the fate of EDN after binding to the cell surface (Figure 7). Radiolabeled enzymes were incubated with KS Y-1 cells for two hours at 37°C. After removing unbound enzyme, the cells were cultured for various times and the amount of protein retained in the cells and released into the medium as intact or degraded protein was determined. Indeed, different patterns of processing were observed for each enzyme. EDN was retained longer inside KS Y-1 cells, decreasing to only about 30% of initial levels over 30 hours. In contrast, intracellular levels of (-4)EDN decreased rapidly to about 40% of initial levels within two hours. Furthermore, (-4)EDN was released into the medium as intact protein, whereas about 20% of EDN was degraded. Taken together, differential processing of the two forms of EDN implies differences in intracellular compartmentalization and/or routing.

### Immunofluorescence analysis of intracellular EDN and (-4)EDN

KS Y-1 cells were incubated with EDN or (-4)EDN for two hours at 37°C and processed for analysis by laser scanning confocal microscopy. Staining was greater in cells incubated with either RNase than in control cells, demonstrating visually the internalization of both enzymes (Figure 8(b) and (c) *versus* (a)). While predominantly nuclear localization of both EDNs was observed, EDN also localized in discrete cytoplasmic granules. Cells incubated with EDN stained more brightly than those treated with (-4)EDN, consistent with the observed greater binding of radiolabeled EDN. Moreover, as observed in the processing experiments, EDN was retained in the cells longer than (-4)EDN when the appearance and disappearance of fluorescent proteins was followed with time (data not shown).

### Conclusions

A major finding in this study is that the peptide extension did not change the overall conformation of native EDN. This indicates that the differences in binding and internalization that were demonstrated with (-4)EDN *versus* EDN are due solely

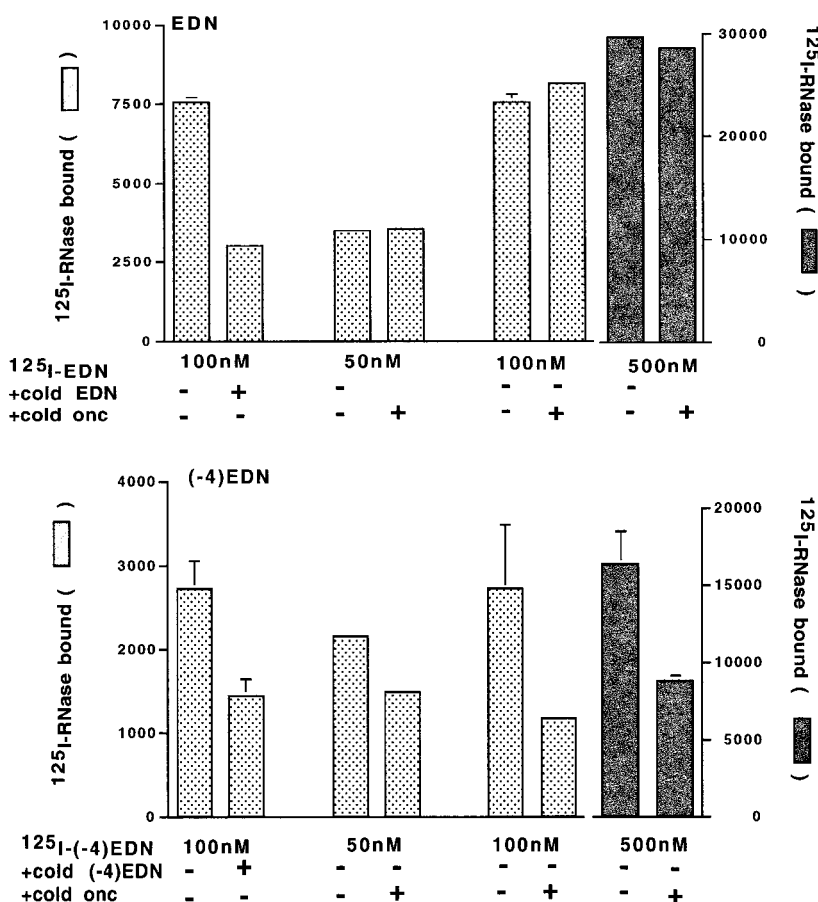


**Figure 6.** Onconase competes with (-4)EDN but not EDN for binding to KS Y-1 cells: 100 nM [<sup>125</sup>I]EDN or [<sup>125</sup>I](-4)EDN were incubated in the presence of a 55-fold or 44-fold molar excess of unlabeled EDN or (-4)EDN, respectively, for two hours on ice as described in Materials and Methods. Additionally, the indicated concentrations of [<sup>125</sup>I]EDN or [<sup>125</sup>I](-4)EDN were incubated with KS Y-1 cells in the absence or the presence of a 100-fold molar excess of unlabeled onconase. The cell-bound radioactivity was determined as described in Materials and Methods.

to the peptide recognition of a cellular marker that alters intracellular processing and/or routing, allowing (-4)EDN to access an intracellular target causing cell death. This is consistent with our previous results showing specific cytotoxicity of (-4)EDN<sup>8,9</sup> and of antibody-targeted EDN.<sup>29</sup> Targeting RNase to kill cells has a counterpart in nature. In bacteria, the colicins E3 and E6 are targeted RNases that cleave the small rRNA and kill susceptible bacteria.<sup>2,30</sup> In this regard, they are structurally and functionally reminiscent of RNase fusion proteins genetically engineered to target and kill diseased cells and tissues.<sup>31</sup> Since (-4)EDN is present in humans and inhibits oocyte maturation, a function not shared by the native enzyme,<sup>5,6</sup> it is the first example of a natural human targeted cytotoxic RNase. Future studies will determine the potential therapeutic use of this peptide-extended EDN and serve as a paradigm for designing other peptide-targeted RNases.

## Materials and Methods

### Crystallization, data collection, and structure refinement

The expression and purification of (-4)EDN has been described.<sup>8</sup> Purified enzyme was pooled and concentrated to 20 mg/ml, with crystallization performed by the hanging-drop vapor diffusion method at 22 °C. Crys-

tal screen I (Hampton Research) was used for the initial screening, whereas the final crystallization condition was 100 mM sodium cacodylate (pH 6.5), 12-16% (w/v) PEG 8 K, 150-200 mM ammonium sulfate, and 12% (v/v) glycerol. The hanging drop was composed of 1 μl of well solution and 2 μl of protein solution. Crystals grew to the size of 0.4-0.7 mm in about ten days. They belong to the orthorhombic space group *P*2<sub>1</sub>2<sub>1</sub>2<sub>1</sub> with the unit cell parameters *a* = 42.14 Å, *b* = 52.56 Å, *c* = 56.63 Å and with *V*<sub>M</sub> = 1.97 Å<sup>3</sup>/Da. It needs to be noted that the crystallographic axes have been defined here according to the usual notation for this space group, but this definition is not consistent with the usage employed for the other structures of EDN.<sup>11,12</sup>

A data set extending to 1.0 Å was collected at 100 K using the ADSC Quantum 4 CCD detector on the synchrotron beamline X9B at the National Synchrotron Light Source, Brookhaven National Laboratory, Upton, New York. Data were integrated and scaled using the HKL2000 program suite.<sup>32</sup> The statistics of data collection are summarized in Table 1.

The structure of (-4)EDN was solved by molecular replacement with the program AMoRe.<sup>33</sup> A search model was provided by the previously solved EDN structure.<sup>11</sup> The fully automated script was run in the resolution range 12-3.0 Å, yielding the position a molecule with a correlation coefficient of 0.285, and an *R*-factor of 46.4%. The model of (-4)EDN was refined using SHELXL<sup>34</sup> at the resolution range of 20.0-1.0 Å. The anisotropic *B*-factors were refined for all atoms except for side-chain atoms in flexible regions and water molecules with high temperature factors. Hydrogen

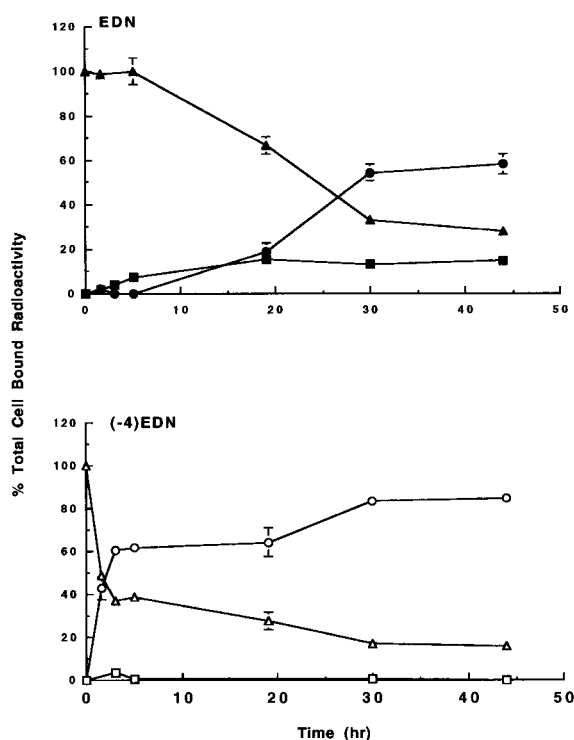


**Figure 7.** Retention and processing of [ $^{125}$ I]EDN and [ $^{125}$ I](-4)EDN bound to KS Y-1 cells. KS Y-1 cells were incubated with 10  $\mu$ g/ml of labeled EDN (filled symbols) or (-4)EDN (open symbols) for two hours at 37°C, washed and then cultured for varying times at 37°C. At the indicated time-points, the amount of protein released into the medium either intact (circles) or degraded (squares), or the amount still retained by the cells (triangles) was determined as described in Materials and Methods. Values shown are means of triplicate determinations. Standard errors of the means are shown when they are greater than the symbol. This is one of two representative experiments.

atoms for protein molecules were added at the final stage of refinement with the HFIX command in SHELXL. The model was rebuilt with the program O<sup>35</sup> using both  $2F_o - F_c$  and  $F_o - F_c$  maps.

The geometrical properties of the model were assessed with the program PROCHECK<sup>36</sup> and the secondary structure elements were assigned by the program PROMOTIF.<sup>37</sup> The surface charge potential was calculated by GRASP<sup>38</sup> and this program was used to generate surface displays. Other Figures were prepared with MOLSCRIPT<sup>39</sup> or Bobscrip<sup>40</sup> and rendered with Raster3D.<sup>41</sup>

#### Ribonuclease assay

The RNase activity of EDN and (-4)EDN was determined at 37°C by monitoring the formation of perchloric acid-soluble nucleotides.<sup>42</sup> The following buffer was used (final volume of 0.3 ml); 0.16 M Tris-HCl (pH 7.5), 1.6 mM EDTA, 0.2 mg/ml of human serum albumin (HSA) (Sigma, St. Lewis, MO). Final tRNA concentrations ranged from 0.1 to 1.0 mg/ml and incubation time was 15 minutes. Each assay was repeated at least

twice and the data pooled. For those assays in which the pH was varied (data not shown), the following buffers were used: for pH 6 and 6.5; 30 mM MES (pH 6.0 or 6.5), containing 0.2 mg/ml of HSA; for pH 8.0, 0.16 M Tris-HCl (pH 8.0), 1.6 mM EDTA, 0.2 mg/ml of HSA. The final tRNA concentration was 0.3 mg/ml.

#### Protein iodination

NaPO<sub>4</sub> (0.2 M, pH 7.5, 50  $\mu$ l) was added to 1 mCi of  $^{125}$ I (Amersham Pharmacia Biotech, Piscataway, NJ) and 25  $\mu$ l of this was added to each of 0.25 mg of EDN or (-4)EDN (stock concentration, 1 mg/ml). This was followed by the addition of freshly prepared chloramine T (11.5  $\mu$ l of a 2 mg/ml stock solution in water) and the mixtures were incubated for five minutes at room temperature. The incubation was continued for an additional minute after the addition of 23  $\mu$ l of sodium metabisulfite (stock solution, 2 mg/ml in water). Each mixture was then applied to a PD10 column (Amersham Pharmacia Biotech, Piscataway, NJ) equilibrated and eluted with PBS containing 0.1% (w/v) bovine serum albumin (BSA). The specific activity was  $6.8 \times 10^5$  and  $8.8 \times 10^5$  cpm/ $\mu$ g protein for (-4)EDN and EDN, respectively, for all experiments unless otherwise noted.

#### Binding assay

KS Y-1 cells, Kaposi's sarcoma-derived neoplastic endothelial cells,<sup>24</sup> were plated at 20,000 cells per well of a 48-well plate two days before treatment. Before use, the cells were rinsed and 100  $\mu$ l of fresh medium added. Where indicated, unlabeled EDN, (-4)EDN, or onconase was added 15 minutes prior to the addition of  $^{125}$ I-labeled protein. The cells were incubated for two hours on ice, then washed twice with ice-cold PBS containing 0.1% BSA before 100  $\mu$ l of 0.1 M NaOH was added to solubilize the cells. After incubation at 37°C for 30 minutes, the contents of the wells were transferred to counting vials and the radioactivity was measured with a gamma counter. Duplicates from at least three experiments were pooled. Non-specific binding was determined by using a 100-fold excess of unlabeled EDN, (-4)EDN, or onconase (kindly provided by Alfacell Corp., Bloomfield, NJ). Scatchard analysis of the (-4)EDN binding data was performed using PRISM 3.

#### Retention and processing of EDN and (-4)EDN bound to KS Y-1 cells

KS Y-1 cells were plated at 9000 cells/well of a 96-well microtiter plate (0.1 ml final volume) one day before treatment. Cells were incubated in triplicate with 10  $\mu$ g/ml of [ $^{125}$ I]EDN or [ $^{125}$ I](-4)EDN for two hours at 37°C. After washing to remove the unbound protein, the cells were cultured for varying periods ranging from two hours to 44 hours in 200  $\mu$ l of culture medium at 37°C in a humidified CO<sub>2</sub> incubator. At each time-point, 80  $\mu$ l of supernatant was collected and counted (represents total released protein). To determine whether the protein found in the supernatant was degraded or intact, another aliquot of the supernatant was treated with an equal volume of cold 3.25% (w/v) phosphotungstate in 5% (v/v) HCl, with 0.01 mg/ml of BSA as the carrier protein. After centrifugation for 15 minutes in a microcentrifuge at top speed, the supernatant was counted (represents degraded protein). Intact protein was found in the pellet. The cells remaining in the well were solubil-

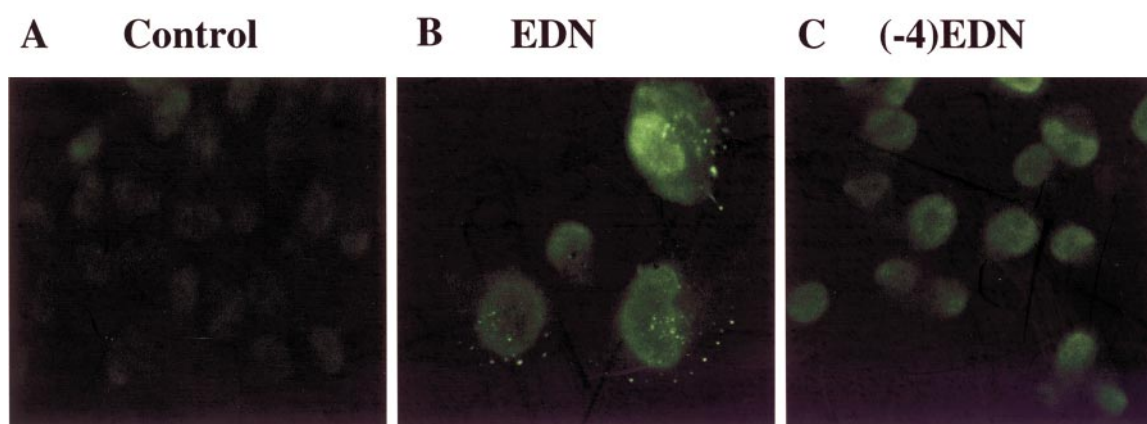


**Figure 8.** Fluorescence studies of the internalization of EDN and (-4)EDN into KS Y-1 cells. KS Y-1 cells were treated with 100  $\mu\text{g}/\text{ml}$  of EDN or (-4)EDN for two hours at 37°C, washed with PBS, fixed with paraformaldehyde, and permeabilized. Cells were then incubated with anti-EDN serum followed by incubation with Alexa-labeled goat anti-rabbit secondary antibody. The cells were examined under a laser scanning confocal microscope.

ized with 0.1 M NaOH (represents retained protein). Thus, at each time-point, the percentages of retained protein and released protein were determined, the released protein being subdivided into intact and degraded protein.

#### Immunofluorescence studies

KS Y-1 cells (25,000 cells) were plated in two-well coverglass chambers (Nalge NUNC International, Naperville, IL) pretreated with fetal bovine serum (FBS) for at least two hours at room temperature. The cells were grown for two days at 37°C in a humidified CO<sub>2</sub> incubator to allow attachment of the cells to the glass coverslip. The cells were then washed with PBS and incubated in complete medium containing 100  $\mu\text{g}/\text{ml}$  of EDN or (-4)EDN at 37°C. After two hours, the cells were washed with PBS, fixed with 3.7% (v/v) paraformaldehyde, permeabilized with cold methanol, and blocked with 4% (w/v) milk/2% BSA in PBS for 30 minutes. EDN antisera (1:500 dilution) preabsorbed with KS Y-1 cells was added to each well and the incubation continued for 60 minutes at room temperature. This was followed by washing (three times) with 1% BSA in PBS and the addition of Alexa-labeled anti-rabbit antibody at the manufacturer's recommended dilution (Molecular Probes, Inc., Eugene, OR). After incubation for 60 minutes in the dark, the cells were rinsed with 1% BSA in PBS (three times) and viewed with a laser scanning confocal microscope (Meridian Insight Plus, Meridian, MI).

#### Protein Data Bank accession code

The final coordinates and the structure factors have been deposited with the RCSB Protein Data Bank under accession code 1K2A.

#### Acknowledgments

We thank Dr Z. Dauter for his assistance in data collection on beamline X9B at the National Synchrotron Light Source, Brookhaven National Laboratory, Susan Kenney for her assistance with confocal microscopy, Dale Ruby for excellent technical support, and the continued support and interest of Dr Edward A. Sausville. This project has been funded in whole or in part with federal funds from the National Cancer Institute, National Institutes of Health, under contract no. NO1-CO-56000. The content of this publication does not necessarily reflect the views or policies of the Department of Health and Human Services, nor does mention of trade names, commercial products, or organizations imply endorsement by the US Government.

#### References

1. Schein, C. H. (1997). From housekeeper to microsurgeon: the diagnostic and therapeutic potential of ribonucleases. *Nature Biotechnol.* **15**, 529-536.
2. Youle, R. J., Newton, D., Wu, Y. N., Gadina, M. & Rybak, S. M. (1993). Cytotoxic ribonucleases and chimeras in cancer therapy. *Crit. Rev. Ther. Drug Carrier Syst.* **10**, 1-28.
3. Benner, S. A. & Allemann, R. K. (1989). The return of pancreatic ribonucleases. *Trends Biochem. Sci.* **14**, 396-397.
4. Domachowske, J. B., Bonville, C. A., Dyer, K. D. & Rosenberg, H. F. (1998). Evolution of antiviral activity in the ribonuclease A gene superfamily: evidence for a specific interaction between eosinophil-derived neurotoxin (EDN/RNase 2) and respiratory syncytial virus. *Nucl. Acids Res.* **26**, 5327-5332.
5. Sakakibara, R., Hashida, K., Tominaga, N., Sakai, K., Ishiguro, M., Imamura, S. *et al.* (1991). A putative mouse oocyte maturation inhibitory protein from urine of pregnant women: N-terminal sequence homology with human nonsecretory ribonuclease. *Chem. Pharm. Bull. (Tokyo)*, **39**, 146-149.

6. Sakakibara, R., Hashida, K., Kitahara, T. & Ishiguro, M. (1992). Characterization of a unique nonsecretory ribonuclease from urine of pregnant women. *J. Biochem. (Tokyo)*, **111**, 325-330.
7. Arap, W., Pasqualini, R. & Ruoslahti, E. (1998). Cancer treatment by targeted drug delivery to tumor vasculature in a mouse model. *Science*, **279**, 377-380.
8. Newton, D. L. & Rybak, S. M. (1998). Unique recombinant human ribonuclease and inhibition of Kaposi's sarcoma cell growth. *J. Natl Cancer Inst.* **90**, 1787-1791.
9. Newton, D. L., Kaur, G., Rhim, J. S., Sausville, E. A. & Rybak, S. M. (2001). RNA damage and inhibition of neoplastic endothelial cell growth: effects of human and amphibian ribonucleases. *Radiat. Res.* **155**, 171-174.
10. Lunardi-Iskandar, Y., Bryant, J. L., Zeman, R. A., Lam, V. H., Samaniego, F., Besnier, J. M. *et al.* (1995). Tumorigenesis and metastasis of neoplastic Kaposi's sarcoma cell line in immunodeficient mice blocked by a human pregnancy hormone. *Nature*, **375**, 64-68.
11. Mosimann, S. C., Newton, D. L., Youle, R. J. & James, M. N. (1996). X-ray crystallographic structure of recombinant eosinophil-derived neurotoxin at 1.83 Å resolution. *J. Mol. Biol.* **260**, 540-552.
12. Leonidas, D. D., Boix, E., Prill, R., Suzuki, M., Turton, R., Minson, K. *et al.* (2001). Mapping the ribonucleolytic active site of eosinophil-derived neurotoxin (EDN). High resolution crystal structures of EDN complexes with adenylic nucleotide inhibitors. *J. Biol. Chem.* **276**, 15009-15017.
13. Ramakrishnan, C. & Ramachandran, G. N. (1965). Stereochemical criteria for polypeptide and protein chain conformations. II Allowed conformation for a pair of peptide units. *Biophys. J.* **5**, 909-933.
14. Esposito, L., Vitagliano, L., Sica, F., Sorrentino, G., Zagari, A. & Mazzarella, L. (2000). The ultrahigh resolution crystal structure of ribonuclease A containing an isoaspartyl residue: hydration and stereochemical analysis. *J. Mol. Biol.* **297**, 713-732.
15. Svensson, L. A., Sjölin, L., Gilliland, G. L., Finzel, B. C. & Wlodawer, A. (1986). Multiple conformations of amino acid residues in ribonuclease A. *Proteins: Struct. Funct. Genet.* **1**, 370-375.
16. Nachman, J., Miller, M., Gilliland, G. L., Carty, R., Pincus, M. & Wlodawer, A. (1990). Crystal structure of two covalent nucleoside derivatives of ribonuclease A. *Biochemistry*, **29**, 928-937.
17. Wlodawer, A. (1985). Structure of bovine pancreatic ribonuclease by X-ray and neutron diffraction. In *Biological Macromolecules and Assemblies* (Jurnak, F. A. & McPherson, A., eds), pp. 393-439, John Wiley & Sons, New York.
18. Birdsall, D. L. & McPherson, A. (1992). Crystal structure disposition of thymidylic acid tetramer in complex with ribonuclease A. *J. Biol. Chem.* **267**, 22230-22236.
19. Zegers, I., Maes, D., Dao-Thi, M. H., Poortmans, F., Palmer, R. & Wyns, L. (1994). The structures of RNase A complexed with 3'-CMP and d(CpA): active site conformation and conserved water molecules. *Protein Sci.* **3**, 2322-2339.
20. Leonidas, D. D., Shapiro, R., Irons, L. I., Russo, N. & Acharya, K. R. (1997). Crystal structures of ribonuclease A complexes with 5'-diphosphoadenosine 3'-phosphate and 5'-diphosphoadenosine 2'-phosphate at 1.7 Å resolution. *Biochemistry*, **36**, 5578-5588.
21. Leonidas, D. D., Shapiro, R., Irons, L. I., Russo, N. & Acharya, K. R. (1999). Toward rational design of ribonuclease inhibitors: high-resolution crystal structure of a ribonuclease A complex with a potent 3',5'-pyrophosphate-linked dinucleotide inhibitor. *Biochemistry*, **38**, 10287-10297.
22. Fedorov, A. A., Joseph-McCarthy, D., Fedorov, E., Sirakova, D., Graf, I. & Almo, S. C. (1996). Ionic interactions in crystalline bovine pancreatic ribonuclease A. *Biochemistry*, **35**, 15962-15979.
23. Sorrentino, S., Glitz, D. G. J., Hamann, K. J., Loegering, D. A., Checkel, J. L. & Gleich, G. J. (1992). Eosinophil-derived neurotoxin and human liver ribonuclease. Identity of structure and linkage of neurotoxicity to nuclease activity. *J. Biol. Chem.* **267**, 14859-14865.
24. Lunardi-Iskandar, Y., Gill, P., Lam, V. H., Zeman, R. A., Michaels, F., Mann, D. L. *et al.* (1995). Isolation and characterization of an immortal neoplastic cell line (KS Y-1) from AIDS-associated Kaposi's sarcoma. *J. Natl Cancer Inst.* **87**, 974-981.
25. Saxena, S. K., Rybak, S. M., Winkler, G., Meade, H. M., McGray, P., Youle, R. J. & Ackerman, E. J. (1991). Comparison of RNases and toxins upon injection into *Xenopus* oocytes. *J. Biol. Chem.* **266**, 21208-21214.
26. Wu, Y. N., Saxena, S. K., Ardel, W., Gadina, M., Mikulski, S. M., DeLorenzo, C. *et al.* (1995). A study of the intracellular routing of cytotoxic ribonucleases. *J. Biol. Chem.* **270**, 17476-17481.
27. Nitta, K. (2001). Assay for antitumor and lectin activity in RNase homologs. *Methods Mol. Biol.* **160**, 363-373.
28. Wu, Y. N., Mikulski, S. M., Ardel, W., Rybak, S. M. & Youle, R. J. (1993). Cytotoxic ribonuclease: a study of the mechanism of onconase cytotoxicity. *J. Biol. Chem.* **268**, 10686-10693.
29. Newton, D. L., Nicholls, P. J., Rybak, S. M. & Youle, R. J. (1994). Expression and characterization of recombinant human eosinophil-derived neurotoxin and eosinophil-derived neurotoxin-anti-transferrin receptor sFv. *J. Biol. Chem.* **269**, 26739-26745.
30. James, R., Kleanthous, C. & Moore, G. R. (1996). The biology of E colicins: paradigms and paradoxes. *Microbiology*, **142**, 1569-1580.
31. Rybak, S. M. & Newton, D. L. (1999). Immunoenzymes. In *Antibody Fusion Proteins* (Chamow, S. M. & Ashkenazi, A., eds), pp. 53-110, John Wiley & Sons, New York.
32. Otwinowski, Z. & Minor, W. (1997). Processing of X-ray diffraction data collected in oscillation mode. *Methods Enzymol.* **276**, 307-326.
33. Navaza, J. (1994). AMoRe: an automated package for molecular replacement. *Acta Crystallog. sect. A*, **50**, 157-163.
34. Sheldrick, G. M. & Schneider, T. R. (1997). SHELXL: high-resolution refinement. *Methods Enzymol.* **277**, 319-343.
35. Jones, T. A. & Kieldgaard, M. (1997). Electron-density map interpretation. *Methods Enzymol.* **277**, 173-208.
36. Laskowski, R. A., MacArthur, M. W., Moss, D. S. & Thornton, J. M. (1993). PROCHECK: program to check the stereochemical quality of protein structures. *J. Appl. Crystallog.* **26**, 283-291.
37. Hutchinson, E. G. & Thornton, J. M. (1996). PROMOTIF - a program to identify and analyze structural motifs in proteins. *Protein Sci.* **5**, 212-220.

38. Nicholls, A. (1992). *GRASP: Graphical Representation and Analysis of Surface Properties*, Columbia University, New York, NY.
39. Kraulis, P. J. (1991). MOLSCRIPT: a program to produce both detailed and schematic plots of protein structures. *J. Appl. Crystallog.* **24**, 946-950.
40. Esnouf, R. M. (1999). Further additions to MolScript version 1.4, including reading and contouring of electron-density maps. *Acta Crystallog. sect. D*, **55**, 938-940.
41. Meritt, E. A. & Murphy, M. E. P. (1994). Raster3D version 2.0. A program for photorealistic molecular graphics. *Acta. Crystallog. sect. D*, **50**, 869-873.
42. Newton, D. L., Boque, L., Wlodawer, A., Huang, C. Y. & Rybak, S. M. (1998). Single amino acid substitutions at the N-terminus of a recombinant cytotoxic ribonuclease markedly influence biochemical and biological properties. *Biochemistry*, **37**, 5173-5183.

*Edited by R. Huber*

(Received 24 September 2001; received in revised form 6 January 2002; accepted 7 January 2002)